Research Article | Vol. 30, No. 24 / 21 Nov 2022 / Optics Express 43118
Optics EXPRESS

E-, S-, C- and L-band coherent transmission with a multistage discrete Raman amplifier

PRATIM HAZARIKA,[1,*] MINGMING TAN,[1] ALEKSANDR DONODIN,[1] SHABNAM NOOR,[1] IAN PHILLIPS,[1] PAUL HARPER,[1] JEFFERY S. STONE,[2] MING JUN LI,[2] AND WLADEK FORYSIAK[1]

[1]Aston Institute of Photonic Technologies, Aston University, Birmingham B4 7ET, UK
[2]Corning Incorporated, 1 Riverfront Plaza, Corning, NY 14831, USA
[*]p.hazarika@aston.ac.uk

Abstract: We report for the first time an ultra-wideband coherent (UWB) WDM transmission over a 70 km standard single mode fibre (SSMF) solely using a multistage discrete Raman amplifier (DRA) over the E-, S-, C- and L-bands of the optical window. The amplifier is based on a split-combine approach of spectral bands enabling signal amplification from 1410-1605 nm over an optical bandwidth of 195 nm (25.8 THz). The proposed amplifier was characterized with 143 channelized amplified spontaneous emission (ASE) dummy channels in the S-, C- and L-bands and 4 laser sources in the E-band (1410–1605 nm). The amplification results show an average gain of 14 dB and a maximum noise figure (NF) of 7.5 dB over the entire bandwidth. Coherent transmission with the proposed amplifier was performed using a 30 Gbaud PM-16-QAM channel coupled with the ASE channels over a 70 km SMF. The ultra-wideband transmission using the tailored multistage DRA shows transmission bandwidth of 195 nm with a maximum Q^2 penalty of ~4 dB in E- and S-band, and ~2 dB in C- and L-band.

1. Introduction

The ever-increasing demand on data [1,2] with each passing year has inspired the scientific community to consider new technologies for high data throughput optical fibre communication systems. Novel approaches such as signal transmission in the spatial domain [3,4] are powerful tools to meet such demands. However, establishment of such a network requires expensive capital expenditure (CAPEX) and complex system integration when targeted towards a large scale deployment [5]. An alternative approach can be a full scale exploitation of the optical windows in a single mode fibre (SMF), also known as multiband transmission (MBT) [6]. A combination of MBT with higher order modulation formats can be a cost-effective network solution enabling full utilization of an already existing fibre infrastructure.

However, deployment of a MBT architecture requires upgrade at both the node and operator level in the existing network for high data throughput. Moving from the conventional C-band towards a MBT architecture necessitates the design and development of new amplifiers capable of signal amplification in the unused spectral bands [7], as the existing erbium doped fibre amplifier (EDFA) in the fibre network can support only in the C- and L-bands [8]. Amplification with rare-earth materials such as Bismuth, Thulium and Praseodymium can be a good choice for signal amplification in for O-, E- and S-band with numerous experimental demonstrations showing the use of such amplifiers in a transmission system [9–12]. Another interesting amplifier enabling multiband (MB) signal amplification is the semiconductor optical amplifier (SOA) with experimental demonstrations showing ultra-wideband (UWB) amplification of ~100 nm [13]

#474327 https://doi.org/10.1364/OE.474327
Journal © 2022 Received 29 Aug 2022; revised 20 Oct 2022; accepted 24 Oct 2022; published 8 Nov 2022

Optics EXPRESS

covering the C- and L-band. Net throughputs of 178.08 Tb/s [14] and 244.3 Tb/s [15] have been achieved with transmission experiments in the S-, C- and L-band, using hybrid combinations of doped fibre amplifiers and distributed Raman amplifiers, and together with launch power optimization, a net data throughput of 150.3 Tb/s has also been reported [16]. In addition to the above mentioned amplifiers, a separate category of amplifier with high potential for UWB signal amplification is the discrete Raman amplifier (DRA), with recent experimental demonstration showing an amplification bandwidth of ~150 nm over the S-, C- and L-bands, with a net gain of 15 dB and a maximum noise figure (NF) of ~8 dB, using a dual stage DRA [17]. In terms of maximum achievable gain, a record gain of 27 dB with an average NF of 5.8 dB using dual-stage DRA has also been reported [18]. In our previous works, we reported 10G NRZ transmission with a multistage DRA over a bandwidth of 210 nm and 30 Gbaud PM-16-QAM coherent transmission over a bandwidth of 195 nm with a hybrid BDFA–DRA [19,20]. In this paper, we extend our multistage DRA over a coherent WDM system with PM-16QAM modulating signals over the E- (1410-1457 nm), S- (1470-1520nm), FC- (1530-1565 nm) and L- (1570-1605nm) bands. The multistage DRA was characterized with a fully loaded 143×100 GHz amplified spontaneous emission (ASE) dummy channels in the S-, C- and L-band coupled together with 4 sources in the E-band. Our experimental results show an average gain of 14 dB with a maximum NF of ~7.5 dB across the full optical bandwidth of 195 nm. WDM transmission was performed using a 30 Gbaud PM-16-QAM signal coupled with the dummy channels over a transmission distance of 70 km with standard single mode fibre (SSMF). Our results show a transmission bandwidth of 195 nm (25.8 THz) over a 70km SMF span with a maximum Q^2 penalty of ~4 dB over E- and S-band, and ~2 dB Q^2 penalty over C- and L-band.

2. Multistage discrete Raman amplifier characterization

The developed multistage DRA was characterized using the experimental setup shown in Fig. 1(a). The setup comprises a 143×100 GHz (50 GHz bandwidth) S-, C- and L-band WDM grid and 3 laser diodes at 1411, 1431 and 1451 nm combined with a 30 Gbaud PM-16-QAM signal at 1457nm to encapsulate a target bandwidth ~195 nm (25.83 THz). Altogether, the spectrum comprised 147 WDM slots (1 data channel at 1457 nm, 3 narrow linewidth lasers, and 143 ASE dummy signals) extending from 1410-1605 nm. The S-band channels were generated using a supercontinuum source and a commercial waveshaper followed a thulium- doped amplifier (TDFA) with an operation range of 1470-1520 nm. Guard bands of +/- 2nm in the proximity of 1485 nm and +/- 3nm at 1508 nm were inserted to prevent signal overlap with the 1485 and 1508 nm pumps in the DRA, as previously explained [21]. The S-band signals were coupled with flat channelized C- and L-band ASE signals extending from 1530-1605 nm generated using two C- and L-band EDFAs and two equalizers. The generated S-, C- and L- grid was coupled with the four E-band sources to form an E-, S- C- and L-band WDM grid (Fig. 2(a)). In the E-band we used 4 dummy channels due to the unavailability of ASE source and commercially available WSS for channel shaping and equalization. Nevertheless, we managed to insert our signals at the extreme ends of our target bandwidth to measure the performance of our proposed amplifier. The generated signals were then transmitted through 70 km of SSMF before being amplified in the DRA, resulting in the output spectrum shown in Fig. 2(c). This was done for a standalone transmission and to test our amplifier in a more realistic UWB scenario where the effects of inter-channel stimulated Raman scattering (ISRS) power transfer and wavelength dependent attenuation cause signal degradation [22]. The total input power to the fibre was 19.6 dBm with a power per channel of ~ -2 dBm, and the total SSMF loss was ~14.8 dB across the entire bandwidth.

At the input to the DRA (Fig. 1(a)), a filtered wavelength division multiplexer (FWDM) with passband from (1260-1457 nm) and reflection band from (1464-1620 nm) was used to split the optical signal into two bands, comprising of 1410-1457 nm and 1470-1605 nm, respectively.

Optics EXPRESS

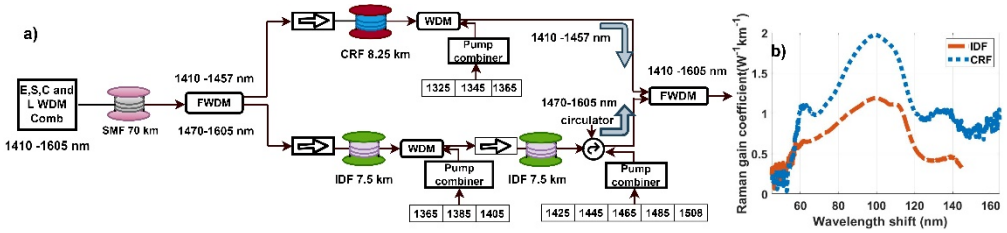

Fig. 1. a) Schematic of the multistage DRA b) Raman gain coefficient of IDF and CRF.

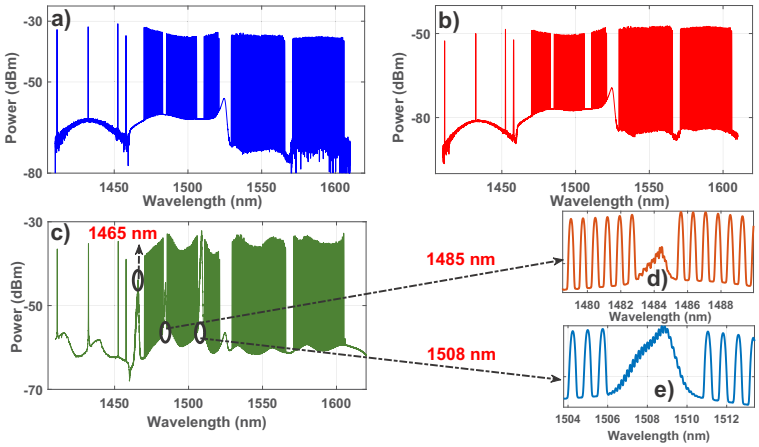

Fig. 2. WDM optical spectrum of the ASE grid a) input to SSMF b) output from SSMF c) amplified output spectrum from the multistage DRA; Rayleigh backscattered spectrum of d) 1485 and e) 1508 nm pumps.

The separated bands were then sent to the multistage DRA for signal amplification of the target bands. Signals from 1410-1457 nm were amplified using 8.25km of a newly developed fibre known as Corning Raman Fibre (CRF) [23,24], backward-pumped using 1325, 1345 and 1365 nm pumps (pump power values of 435, 276 and 168 mW). Correspondingly, 1470-1605 nm signals were amplified using a backward pumped dual-stage DRA, with 7.5 km inverse dispersion fibre (IDF) in each stage. The dual-stage architecture was specifically chosen to minimize the effect of pump-to-signal overlap and pump-to-pump ISRS power transfer [21,25]. A total of 8 pumps at wavelengths of 1365, 1385, 1405, 1425, 1445, 1465, 1485 and 1508 nm, with pump power values of 432, 297, 103, 289, 304, 269, 67 and 172 mW respectively, were used for S-, C- and L-band signal amplification. The experimentally measured Raman gain coefficients of the two different Raman gain fibres (CRF and IDF) are shown in Fig. 1(b) with CRF and IDF having peak Raman gain coefficients (g_r) of ~1.95 $W^{-1}km^{-1}$ and ~1.2 $W^{-1}km$, respectively.

The spectra at the input of SSMF, SSMF output, and the amplified spectrum are shown in Fig. 2(a)–2(c). It can be observed that the signals from 1470-1520 nm (S-band) have a higher noise floor. This is due to the high noise figure (NF) of the TDFA used in the grid generation, as well as a slight tilt of +/-1 dB in the S-band input spectrum (Fig. 2(a)) due to the wavelength dependent loss of the passives used for signal combination. The peaks observed in the vicinity of S-band (Fig. 2(c)) are the Rayleigh backscattered spectra of the 1465, 1485 and 1508 nm pumps, and the zoomed-in spectra of these pumps are shown in Fig. 2(d)–2(e). Appropriate guard bands, as mentioned above, were adopted to prevent overlap between signals and pumps. The non-uniformity in the amplified output optical spectrum (Fig. 2(c)), particularly in S-band is

Optics EXPRESS

partially due to pump power limitation and the limited availability of the commercial pumps, which are only supplied at specific wavelengths. This could be rectified with the improved availability of customized high power pumps at specific wavelength and improved pump power optimization for target gains using established genetic and machine leaning models [26].

Figure 3(a) and 3(b) shows the Gain/ NF and the output optical signal-to-noise ratio (OSNR) of the signals after the multistage Raman amplifier, where the NF was calculated with the calibrated optical spectrum analyser (OSA) power using a standard technique [27]. The net gain profile shown in Fig. 3(a) (red lines with circle markers) has an average gain of 14 dB across the entire bandwidth. The emphasis in this work was to compensate the SSMF span loss for the UWB signals, rather than to obtain a flat gain across the bandwidth. This resulted in a tilted gain profile due to the tilted input power profile (Fig. 2(b)) at the input stage of the DRA. In the S-band region due to the higher SSMF loss and ISRS power transfer in the first stage of the the dual stage DRA, a higher gain of ~16 dB was required to obtain channel powers that were nearly equivalent to those in the C- and L-band, where an average gain of only ~13 dB was required. The corresponding NF for the multistage Raman has an approximate tilt of 1.5 dB with a maximum value of ~7.5 dB across the entire bandwidth. The NF for the four E-band channels has an average value of ~7 dB. However, a slight increase in the NF is expected in the presence of a fully loaded channelized E-band spectrum due to an increased power spectral density. The overall shape of the NF in the S-, C- and L-bands is due to the dual stage architecture adopted here. Athough the gain and NF were measured at interval of 10 nm for the 1470-1605 nm signals, the values obtained are due to the fully loaded channels in the S-, C- and L-bands as shown in Fig. 2(a)–2(c). A higher NF was observed in the S-band, due to the higher S-band attenuation, and the absence of Raman gain at these wavelengths in the second stage of DRA, resulting in S-band attenuation in second stage of the DRA. A slightly lower value of NF can be seen with a value of ~ 6 dB across 1530- 1605 nm signals, due to the ISRS power transfer from the S-band signals to these wavelengths and the lower loss at these wavelengths, resulting in a better input OSNR in the second stage of the DRA. Note, the NF in the E- and S-band could be reduced by replacing CRF and IDF with high Raman gain coefficient (g_r) fibres, ideally with lower E-, S-band loss, and by employing two stage amplification for E- and S-band [25], with appropriate pump wavelengths and powers.

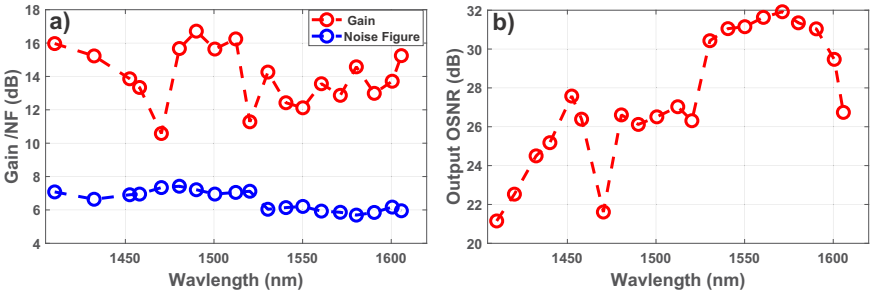

Fig. 3. Multistage Raman amplifier wavelength vs a) Gain/ Noise figure b) Output OSNR

The output OSNR shown in Fig. 3(b) corresponds to the OSNR measured at the output stage of the multistage DRA. The measurements were performed by loading 30 Gbaud PM-16-QAM signals at intervals of 10 nm. In the S-, C- and L-band regions two side channels adjacent to the channel under test (CUT) were turned off and the corresponding OSNR was measured using the 3–point method at a noise bandwidth of 0.1 nm [28]. For the E-band signals there was no requirement for channels to be turned off due to the absence of adjacent channels. Note, for the OSNR measured in a noise bandwidth of 0.1 nm, the equivalent frequency bandwidth of 12.5 GHz is (strictly speaking) valid only at a wavelength of 1548.5 nm (193.6 THz), and should be corrected in a UWB scenario in accordance to [29,30], i.e. the noise spectral density varies as

Optics EXPRESS

$\Delta B = \frac{C}{\lambda^2} * \Delta\lambda$ where, c is the speed of light, $\Delta\lambda$ is the optical spectrum analyzer (OSA) resolution bandwidth which is 0.1 nm and λ is the wavelength of CUT. Our OSNR measurement shows lower output OSNR in the E- and S-band channels with minimum values of ~21 dB at 1410 and 1470 nm. The lower output OSNR of the S-band is partly due to the low input OSNR of the S-band signals due to the high NF of the TDFA and high insertion loss of the WSS used in the ASE grid generation, as seen in the input spectrum of Fig. 2(a). For the 1530-1605 nm signals (C- and L-band), the OSNR varied from 27-31 dB, an improvement attributable to the low NF of the DRA, ISRS power transfer from S- and E-band signals, and the low noise floor of the input ASE grid (Fig. 2(a)).

3. Coherent transmission with multistage Raman amplifier

To evaluate the performance penalty due to our proposed amplifier, coherent transmission was performed over 70 km of SSMF using the DRA inline to compensate for the fibre loss, as illustrated in Fig. 4. The spectrum shown in Fig. 2(a) also corresponds to that used for the coherent transmission. A 30 Gbaud PM-16-QAM signal was generated using a 120 GSa/s digital to analog converter (DAC) and a standard C-band $LiNBO_3$ DP-IQ modulator. Two external cavity laser sources, extending from 1410 -1480 nm and 1480-1620 nm, were required in the transmitter (Tx) section to emulate the WDM carrier from 1410-1605 nm. The modulated signal was then amplified using Tx amplifiers for different wavelength regions, including two EDFAs for C- and L-band (1530-1605 nm), a TDFA for S-band (1470-1520 nm), and an in-house BDFA for E-band (1410-1460 nm) [10]. The modulated signal was then equalized using a variable optical attenuator (VOA) and coupled with the WDM grid using a 90/10 coupler. The total input power to the fibre was 19.6 dBm with a power per channel of ~ -2 dBm. The WDM signals were then passed through 70km of SSMF and the FWDMs with an average loss of ~14.8 dB. The attenuated signals were then amplified using the multistage DRA and passed through a 99/1 tap whose 1% arm was used for the OSNR measurement and spectral monitoring while the remaining 99% arm was passed to the receiver section for data extraction.

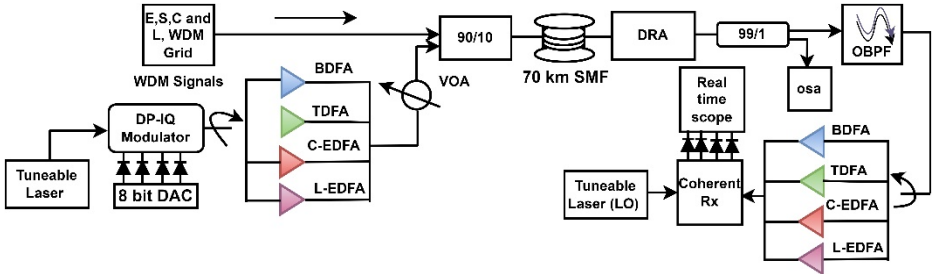

Fig. 4. Experimental setup for E-, S-, C-, L-band coherent WDM transmission.

The receiver (Rx) section comprised an optical band-pass filter (OBPF) for selection of the modulated signal and the corresponding Rx amplifier to provide constant output power for optimal operation of the coherent Rx. The modulated signal was mixed with an external local oscillator and the corresponding traces were captured using an 80 GSa/s (36 GHz analog bandwidth) real time oscilloscope. The detection procedure was followed by standard offline DSP for data recovery on the captured traces. The recorded symbols together with the transmitted symbols were used to estimate the Q^2 factor from the hard decision bit error rate (BER) [31,32].

Optics EXPRESS

4. Results and discussion

Figure 5 show the constellation diagrams of back-to-back (B2B) and received signals after 70 km transmission at 1430, 1500, 1550 and 1605 nm. The constellations for B2B and after 70 km transmission shown below have the best footprint for the 1550 nm signal with minimum noise levels whereas, these larger noise levels were seen for the other bands with a maximum at 1430 nm. The higher noise levels in the B2B constellation plots for 1430, 1500 and 1605 nm signals versus the 1550 nm signals, indicate the performance limitation due to the combined effect of different amplifiers (Tx amplifier, Rx amplifier) and the impact of other standard C-band transceiver components when operated in the E-, S- and L-band. Similarly, for the constellation after 70 km the additional noise level is due to the multistage DRA used for the SSMF loss compensation.

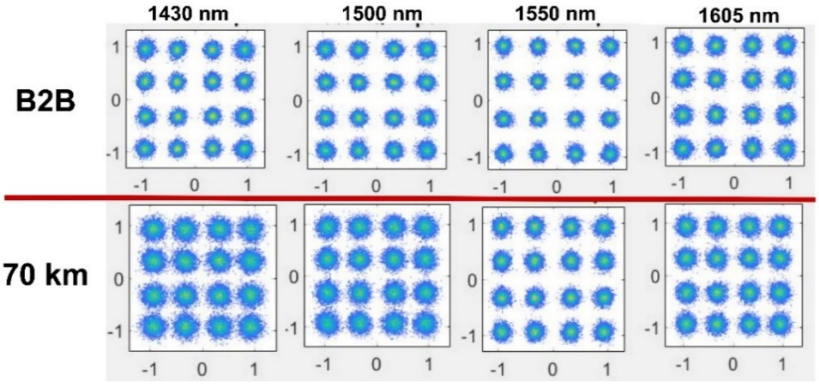

Fig. 5. Constellation diagram for B2B and 70 km transmission for 1430, 1500, 1550 and 1605 nm channels.

The UWB transmission with the multistage stage DRA inline to compensate the fibre loss can be seen below in Figs. 6(a)–6(c). Our transmission results (Q^2 Factor) show degrading B2B performance (blue line with circle marker) for E-band (1410-1457 nm) in comparison to C- and L-band (1470-1605 nm) with a 2.5 dB roll-off. This reduction is primarily due to the use of the standard C-band transceiver components in particular, the I/Q and the polarization imbalance of the C-band transceiver [30]. As for the S-band (1470-1520 nm) a variation of ~ 2 dB was observed with a lowest value of 16 dB at 1470 nm. This performance reduction, specifically towards the shorter wavelengths in the S-band is due to the high NF of the Tx/Rx TDFA, in addition to the I/Q and polarization imbalance. A steady performance of ~ 18 dB can be seen in the C-band (1530-1570 nm) which then degrades down to 16.5 dB at 1605 nm in the L-band, due to the low NF of the C- and L band EDFAs.

The Q^2 factor after 70 km transmission illustrated in Fig. 6(a) (orange line with diamond marker) follows the same trend as the B2B curve for the entire bandwidth. The Q^2 penalty shown in Fig. 6(b) has a maximum of ~2 dB for the C- and L-bands. A higher penalty was observed for the S- and E-band signals, with a maximum of ~4 dB at 1410 and 1470 nm. The average Q^2 penalty in the E- and S-band was ~ 3 dB whereas, for C- and L-band it was ~1.5 dB. The trend in the Q^2 penalty can be largely correlated to the NF and output OSNR of the spectral bands shown in Fig. 2(a)–2(b), where the maximum NF of the DRA was in the E- and S-band region, with an output OSNR <28 dB. Similarly, in the C- and L-band the NF was lower with an OSNR of ~30 dB for all the wavelengths, except 1605 nm. The improved performance in C- and L-band can also be attributed to the ISRS power transfer from the S-band channels in the first DRA stage, subsequently degrading the performance of the S-band signals.

Optics EXPRESS

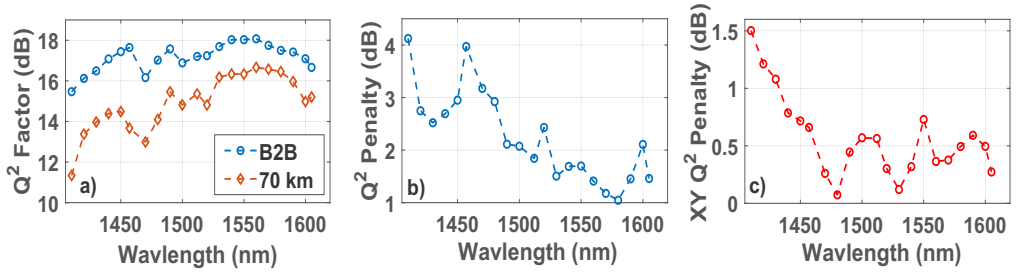

Fig. 6. PM-16-QAM 30 Gbaud transmission; wavelength vs a) Q^2 Factor b) Q^2 Penalty c) XY Q^2 Penalty

As discussed above, an UWB transmission is subject to performance degradation due to I/Q and polarization imbalance, arising from the use of standard C-band modulator and optical hybrid for E-, S- and L-band. To analyze the effects of polarization penalty, we measured XY Q^2 penalty (Fig. 6(c)) which is the difference in the Q^2 factor for X and Y polarization. This penalty was observed to be < 0.6dB for wavelengths > 1480 nm, where a linear increase in this penalty was observed for signals < 1470 nm, with a maximum of 1.5 dB at 1410 nm. In addition to the high NF and low OSNR of the E-band signals, the large polarization imbalance for E-band signals is a major factor in the increase of Q^2 penalty in this spectral region. The overall performance of E- and S-band can be improved by both optimized design of the DRA (design methods mentioned in section 2) and the replacement of C-band components with low loss optical components specifically targeting these bands.

5. Conclusion

We experimentally demonstrated E-, S-, C- and L-band coherent WDM transmission over a 70 km SSMF using an inline multistage DRA to compensate for the fibre loss. The multistage DRA has an average gain of 14 dB with a maximum NF of 7.5 dB over an amplification bandwidth of 195 nm. Moreover, WDM transmission with 30 Gbaud PM-16-QAM shows error-free transmission over 70km of SSMF, despite the gain and NF variations of the multistage DRA, with a maximum Q^2 penalty of ~ 2 dB for C-, L-band, and ~4 dB penalty for E-, S-band signals. To the best of our knowledge this is the broadest coherent transmission bandwidth 195 nm (25.8 THz) demonstrated experimentally solely using a DRA. Based on our experimental results, the discrete Raman amplifier is a potential candidate for signal amplification in MBT systems. Additionally, enhancement in the MBT performance using a multistage DRA can be achieved by proper optimization of pump powers and wavelengths, coupled together with techniques such as split-combine approach of spectral bands.

Funding. Engineering and Physical Sciences Research Council (EP/M009092/1, EP/V000969/1); H2020 Marie Skłodowska-Curie Actions (814276).

Acknowledgement. The authors thank Corning Incorporated for provision of the CRF.

Disclosures. The authors declare no conflicts of interest.

Data availability. The original data for this work is available at Aston Research explorer [33].

References

1. P. J. Winzer, D. T. Neilson, and A. R. Chraplyvy, "Fiber-optic transmission and networking: the previous 20 and the next 20 years [Invited]," Opt. Express **26**(18), 24190 (2018).
2. United Nations Conference on Trade and Development, *DIGITAL ECONOMY REPORT 2019 : Value Creation and Capture - Implications for Developing Countries*. (2019).
3. B. J. Puttnam, G. Rademacher, and R. S. Luís, "Space-division multiplexing for optical fiber communications," Optica **8**(9), 1186 (2021).

Optics EXPRESS

4. D. J. Richardson, J. M. Fini, and L. E. Nelson, "Space-division multiplexing in optical fibres," Nat. Photonics **7**(5), 354–362 (2013).
5. C. Papapavlou, K. Paximadis, and G. Tzimas, "Design and Analysis of a New SDM Submarine Optical Network for Greece," in *International Conference on Information, Intelligence, Systems &Application (IISA)* (IEEE, 2021), pp. 1–8.
6. A. Ferrari, A. Napoli, J. K. Fischer, N. Costa, A. D'Amico, J. Pedro, W. Forysiak, E. Pincemin, A. Lord, A. Stavdas, J. P. F. P. Gimenez, G. Roelkens, N. Calabretta, S. Abrate, B. Sommerkorn-Krombholz, and V. Curri, "Assessment on the Achievable Throughput of Multi-Band ITU-T G.652.D Fiber Transmission Systems," J. Lightwave Technol. **38**(16), 4279–4291 (2020).
7. L. Rapp and M. Eiselt, "Optical Amplifiers for Multi – Band Optical," J. Lightwave Technol. **40**(6), 1579–1589 (2022).
8. A. A. Al-Azzawi, A. A. Almukhtar, A. Dhar, M. C. Paul, H. Ahmad, A. Altuncu, R. Apsari, and S. W. Harun, "Gain-flattened hybrid EDFA operating in C + L band with parallel pumping distribution technique," IET Optoelectron. **14**(6), 447–451 (2020).
9. J. Mirza, S. Ghafoor, N. Habib, F. Kanwal, and K. K. Qureshi, "Performance evaluation of praseodymium doped fiber amplifiers," Opt. Rev. **28**(6), 611–618 (2021).
10. A. Donodin, V. Dvoyrin, E. Manuylovich, L. Krzczanowicz, W. Forysiak, M. Melkumov, V. Mashinsky, and S. Turitsyn, "Bismuth doped fibre amplifier operating in E- and S- optical bands," Opt. Mater. Express **11**(1), 127 (2021).
11. Y. Wang, N. K. Thipparapu, D. J. Richardson, and J. K. Sahu, "Ultra-Broadband Bismuth-Doped Fiber Amplifier Covering a 115-nm Bandwidth in the O and e Bands," J. Lightwave Technol. **39**(3), 795–800 (2021).
12. M. M. Kozak, R. Caspary, and W. Kowalsky, "Thulium-doped fiber amplifier for the S-band," *Proc. 2004 6th Int. Conf. Transparent Opt. Networks 2*, 51–54 (2004).
13. J. Renaudier, A. C. Meseguer, A. Ghazisaeidi, P. Tran, R. R. Muller, R. Brenot, A. Verdier, F. Blache, K. Mekhazni, B. Duval, H. Debregeas, M. Achouche, A. Boutin, F. Morin, L. Letteron, N. Fontaine, Y. Frignac, and G. Charlet, "First 100-nm Continuous-Band WDM Transmission System with 115Tb/s Transport over 100 km Using Novel Ultra-Wideband Semiconductor Optical Amplifiers," in *European Conference on Optical Communication, ECOC* (2017), (1), pp. 1–3.
14. L. Galdino, A. Edwards, W. Yi, E. Sillekens, Y. Wakayama, T. Gerard, W. S. Pelouch, S. Barnes, T. Tsuritani, R. I. Killey, D. Lavery, and P. Bayvel, "Optical Fibre Capacity Optimisation via Continuous Bandwidth Amplification and Geometric Shaping," IEEE Photonics Technol. Lett. **32**(17), 1021–1024 (2020).
15. B. J. Puttnam, R. S. Luís, G. Rademacher, M. Mendez-Astudillio, Y. Awaji, and H. Furukawa, "S-, C- and L-band transmission over a 157 nm bandwidth using doped fiber and distributed Raman amplification," Opt. Express **30**(6), 10011 (2022).
16. F. Hamaoka, M. Nakamura, S. Okamoto, K. Minoguchi, T. Sasai, A. Matsushita, E. Yamazaki, and Y. Kisaka, "Ultra-wideband WDM transmission in S-C- A nd L-bands using signal power optimization scheme," J. Lightwave Technol. **37**(8), 1764–1771 (2019).
17. M. Asif Iqbal, L. Krzczanowicz, I. Phillips, P. Harper, and W. Forysiak, "150 nm SCL-band transmission through 70 km SMF using ultra-wideband dual-stage discrete raman amplifier," in *Optical Fiber Communications Conference and Exhibition (OFC)* (2020), (c), pp. 1–3.
18. S. Liang, S. Jain, L. Xu, K. R. H. Bottrill, N. Taengnoi, M. Guasoni, P. Zhang, M. Xiao, Q. Kang, Y. Jung, P. Petropoulos, and D. J. Richardson, "High Gain, Low Noise, Spectral-Gain-Controlled, Broadband Lumped Fiber Raman Amplifie," J. Lightwave Technol. **39**(5), 1458–1463 (2021).
19. P. Hazarika, M. Tan, A. Donodin, I. Phillips, P. Harper, and W. Forysiak, "210 nm E, S, C and L Band Multistage Discrete Raman Amplifier," in *Optical Fiber Communication Conference (OFC)* Tu3E.2 (2022).
20. A. Donodin, P. Hazarika, M. Tan, V. Dvoyrin, M. Patel, I. Phillips, P. Harper, S. Turitsyn, and W. Forysiak, "195-nm Multi-band amplifier enabled by bismuth-doped fiber and discrete Raman amplification," in *European conference of optical communication (ECOC)* Th2A.1 (2022).
21. M. A. Iqbal, G. Di Rosa, L. Krzczanowicz, I. Phillips, P. Harper, A. Richter, and W. Forysiak, "Impact of pump-signal overlap in S + C+L band discrete Raman amplifiers," Opt. Express **28**(12), 18440 (2020).
22. D. Semrau, R. I. Killey, and P. Bayvel, "A Closed-Form Approximation of the Gaussian Noise Model in the Presence of Inter-Channel Stimulated Raman Scattering," J. Lightwave Technol. **37**(9), 1924–1936 (2019).
23. M. J. Li, S. Li, and D. A. Nolan, "Nonlinear fibers for signal processing using optical Kerr effects," J. Lightwave Technol. **23**(11), 3606–3614 (2005).
24. P. Hazarika, M. Abu-romoh, M. Tan, L. Krzczanowicz, and T. T. Nguyen, "Impact of Chromatic Dispersion in Discrete Raman Amplifiers on Coherent Transmission Systems," in *Optical Fiber Communications Conference and Exhibition (OFC), 2021* (OSA, 2021), pp. 1–3.
25. M. A. Iqbal, L. Krzczanowicz, I. D. Philips, P. Harper, and W. Forysiak, "Noise Performance Improvement of Broadband Discrete Raman Amplifiers Using Dual Stage Distributed Pumping Architecture," J. Lightwave Technol. **37**(14), 3665–3671 (2019).
26. U. C. De Moura, M. A. Iqbal, M. Kamalian, L. Krzczanowicz, F. Da Ros, A. M. R. Brusin, A. Carena, W. Forysiak, S. Turitsyn, and D. Zibar, "Multi-Band Programmable Gain Raman Amplifier," J. Lightwave Technol. **39**(2), 429–438 (2021).

Optics EXPRESS

27. D. Derickson, "Fiber Optic Test and Measurement," in *chapter 13* (Prentince Hall, n.d.) pp. 550–555.
28. "OSNR | ROADM | Signal Power | EXFO," https://www.exfo.com/en/resources/blog/new-iec-standard-osnr-measurements/.
29. I. G. 698. . T-, ITU-*T, Amplified Multichannel DWDM Applications with Single Channel Optical Interfaces* (2007).
30. R. Emmerich, M. Sena, R. Elschner, C. Schmidt-Langhorst, I. Sackey, C. Schubert, and R. Freund, "Enabling S-C-L-band systems with standard C-band modulator and coherent receiver using nonlinear predistortion," J. Lightwave Technol. **40**(5), 1360–1368 (2022).
31. I. D. Phillips, M. Tan, M. F. C. Stephens, M. E. McCarthy, E. Giacoumidis, S. Sygletos, P. Rosa, S. Fabbri, S. T. Le, T. Kanesan, S. K. Turitsyn, N. J. Doran, P. Harper, and A. D. Ellis, "Exceeding the nonlinear-shannon limit using raman laser based amplification and optical phase conjugation," in *Optical Fiber Communication Conference, OFC 2014* (2014), pp. 5–7.
32. A. D. Ellis, M. E. McCarthy, M. A. Z. Al Khateeb, M. Sorokina, and N. J. Doran, "Performance limits in optical communications due to fiber nonlinearity," Adv. Opt. Photonics **9**(3), 429 (2017).
33. P. Hazarika, M. Tan, A. Donodin, S. Noor, I. Phillips, P. Harper, J. S. Stones, M. J. Li, and W. Forysiak, "E-, S-, C- and L-band coherent transmission with multistage discrete Raman amplifier," Research Data (2022). https://doi.org/10.17036/researchdata.aston.ac.uk.00000587